NASA TECHNICAL NOTE

NASA TN D-4631

C. 1

NASA TN D-4631

AN EXPERIMENTAL STUDY OF FLAME PROPAGATION IN SUPERSONIC PREMIXED FLOWS OF HYDROGEN AND AIR

by Griffin Y. Anderson and Allen R. Vick

Langley Research Center
Langley Station, Hampton, Va.

NATIONAL AERONAUTICS AND SPACE ADMINISTRATION • WASHINGTON, D. C. • JUNE 1968

NASA TN D-4631

AN EXPERIMENTAL STUDY OF FLAME PROPAGATION IN SUPERSONIC PREMIXED FLOWS OF HYDROGEN AND AIR

By Griffin Y. Anderson and Allen R. Vick

Langley Research Center
Langley Station, Hampton, Va.

NATIONAL AERONAUTICS AND SPACE ADMINISTRATION

For sale by the Clearinghouse for Federal Scientific and Technical Information
Springfield, Virginia 22151 – CFSTI price $3.00

AN EXPERIMENTAL STUDY OF FLAME PROPAGATION IN SUPERSONIC PREMIXED FLOWS OF HYDROGEN AND AIR

By Griffin Y. Anderson and Allen R. Vick
Langley Research Center

SUMMARY

The results of an experimental study of a Mach 1.5 free jet of hydrogen-air mixture ignited by a coaxial, hot gas, pilot jet are presented. This configuration produces an approximately conical average flame surface propagating from the pilot jet into the unburned, supersonic mixture. Flash schlieren, direct, and time schlieren photographic observations of the flame and flow field are discussed for mixtures up to 1.3 times stoichiometric with stagnation temperatures of 300° K and 450° K. Flame cone half-angle measured from time schlieren photographs is found to increase rapidly with equivalence ratio to a maximum at 0.8 times stoichiometric and remain approximately constant thereafter. The maximum flame angle is approximately 9.2° for mixture stagnation temperature of 300° K and decreases to about 7.4° with an increase in temperature to 450° K. Unlike maximum flame angle, the computed velocity normal to the average flame surface or flame-propagation velocity increases with increasing stagnation temperature. Relative values of flame-propagation velocity computed from flame angles measured in supersonic mixtures for hydrogen, methane, ethane, and ethylene were found to be similar to relative laminar burning velocity data for these fuels.

INTRODUCTION

The desire to operate a fixed-geometry ramjet engine over a broad speed range leads to consideration of the problems involved in extending the operation of a supersonic combustor toward low flight Mach numbers. Principal among these problems is the requirement to establish and propagate combustion throughout an initially supersonic flow that is too cold to autoignite. Besides temperature level, other factors such as nonuniform fuel distribution, pressure gradients, and the presence of walls may play an important part in establishing the ignition requirements and the means necessary to maintain and spread combustion in a practical combustor. As a simplified approach to this complex problem, an experimental study of flame propagation in a supersonic premixed free jet of hydrogen and air has been conducted. References 1 to 3 report the findings of an earlier study under experimental conditions somewhat similar to those of

the present study. The present study was undertaken both to confirm in a large-scale apparatus the experimental observations with hydrogen of references 1 to 3 and to extend the range of combustion conditions studied to include fuel-rich mixtures and uncontaminated heated mixtures. Also, attention was directed to examining schlieren photography as a means of recording flame behavior and to determining, in at least a qualitative manner, the steadiness of the combustion observed.

SYMBOLS

c_p	pressure coefficient defined in equation (A15), dimensionless
f	camera aperture, dimensionless
H_2	hydrogen molecule
M	flow Mach number, dimensionless
$\mathcal{m}$	molecular weight, grams/mole
N_2	nitrogen molecule
n	equation index to account for lean and rich fuel-air mixtures, $n = 0$ for $\phi \leqq 1$; $n = 1$ for $\phi > 1$
O_2	oxygen molecule
p	static pressure, atmospheres
T	static temperature, ^{o}Kelvin
ΔT_c	combustion temperature rise, ^{o}Kelvin
u_F	burning velocity of references 1 and 3 defined in equation (1), meters/second
V	flow velocity, meters/second
v_n	component of flow velocity normal to average flame surface, meters/second
x	axial distance, meters

y	radial distance, meters
α	angle between local flow direction and center line immediately upstream of flame, degrees
γ	ratio of specific heats, dimensionless
η	pressure rise parameter, dimensionless
θ	angle between average flame cone surface and flow center line, degrees
ρ	density, kilograms/meter^3
ϕ	equivalence ratio defined as fuel-air ratio divided by stoichiometric value, dimensionless

Subscripts:

b	burned gas downstream of flame
u	unburned gas upstream of flame
0	nozzle exit plane conditions or free-stream conditions
1	conditions upstream of flame
cp	indicates value for constant pressure process

APPARATUS

The experimental apparatus for this study consists of a hydrogen injector, mixing plenum, and supersonic nozzle shown schematically in figure 1. Heated dry air with stagnation temperature up to 500° K is supplied to the hydrogen injector station from a high pressure supply by a 5.8-meter length of straight pipe approximately 36 centimeters in inside diameter. Ambient temperature hydrogen is introduced by an injector consisting of ten radial fingers spaced evenly around the circumference of the air supply pipe. Each injection finger extends within 1 centimeter of the pipe center line and has nine holes located along its downstream side. The injector hole diameter and spacing were selected so that the ratio of injection hole area to duct cross-section area is a

constant in the annular region fueled by each group of holes at a given radius. Since the injection holes operate choked, this method of injector area distribution provides the correct radial fuel distribution, if uniform air velocity across the pipe approaching the injector is assumed. With this design, fuel must spread radially and circumferentially a distance on the order of the maximum hole spacing rather than the pipe diameter in order to achieve a uniform mixture at the nozzle.

The mixing plenum is a straight pipe section the same diameter as the air supply pipe. The length of the mixing plenum is approximately 1.3 meters or more than 400 times the diameter of the largest fuel injection hole. At its downstream end the mixing plenum fairs into an annular nozzle formed by a 15-centimeter inside diameter pipe and a conical centerbody with 10^{o} half-angle. Pitot and static-pressure surveys in the nozzle exit plane with air only indicate an essentially uniform exit Mach number of 1.47, but since the nozzle centerbody is conical, the flow direction must vary from parallel to the center line at the outer edge of the nozzle to a 10^{o} slope toward the center line along the surface of the centerbody. At all flow conditions a shock starting from the tip of the centerbody turns the flow streamline following the surface of the centerbody parallel to the center line as it leaves the nozzle. Some variation in Mach number, static pressure, and flow direction exists downstream of this shock, but the effect of this nonuniformity on the flame propagation observations of this study are thought to be small.

The nozzle centerbody contains a small air-hydrogen-oxygen burner which supplies hot gas to ignite the main flow of hydrogen-air mixture. In the nozzle centerbody, hydrogen and air are mixed and burned at $\phi \approx 4$. These homogeneous fuel-rich combustion products are supplied to the end of the nozzle centerbody where sufficient oxygen is added to make the overall pilot gas flow approximately stoichiometric. Details of the end of the centerbody are shown to scale in the insert of figure 1. The pilot gas issues from the tip of the nozzle centerbody along the center line of the nozzle as a mixing, reacting, high-temperature jet with a high subsonic Mach number at the same static pressure as the surrounding supersonic flow. Pilot gas flow rates of approximately 2.5, 0.30, and 1.8 grams/second for air, hydrogen, and oxygen, respectively, were used for the greater part of the experimental program. No difference in flame shape was detected at pilot flows twice these values.

Instrumentation includes metering of all gas flows using orifice plates with associated pressure transducers and thermocouples. The flow field and flame propagation were recorded with schlieren, direct, and schlieren motion-picture photography. The schlieren system used for single-frame photographs is a single-pass system with a 30-centimeter-diameter field of view and a mercury arc light source capable of either flash or continuous operation. The schlieren image is recorded by a type K-24 air reconnaissance camera which produces a large negative (approximately 13.5 centimeters

by 14 centimeters) suitable for direct study without enlargement by printing or projection. Flash exposures are obtained with a focal-plane cover curtain, and time exposures are recorded with the continuous light source and a 1/450-second focal-plane shutter. Direct photographs of the flame emission are also recorded by a K-24 camera equipped with a 178-millimeter focal length, f2.5 lens. Exposures of 1/75 second using a focal-plane shutter and up to 10 seconds using a focal-plane cover curtain were required. Schlieren movies were recorded from a double pass schlieren system with a 60-centimeter field of view. The system employs a 16-millimeter Fastax camera and synchronous light source (mercury arc discharge) to obtain framing rates up to 1000 frames per second. Film with an ASA exposure index of 200 was used for all photography with standard development processing.

In a typical experiment the air supply pressure was adjusted with the air flowing to a predetermined value for the target equivalence ratio of the run. Hydrogen supply pressure was adjusted to a corresponding value without flow. The pilot was then ignited, and main hydrogen was injected for a timed interval of 8 to 30 seconds during which photographs and flow data were recorded. No attempt was made to readjust either the main air or hydrogen flow during the period of hydrogen injection. Instead, pressure and flow data from early shakedown runs were used to compute tables of air and hydrogen supply pressure as a function of mixture equivalence ratio and stagnation temperature with a nozzle exit static pressure of 1 atmosphere (where 1 atmosphere equals 1×10^5 newtons/meter^2). By presetting supply pressures in this manner, nozzle exit static pressure was generally held within ± 0.05 atmosphere and target equivalence ratio achieved within ± 0.1.

RESULTS AND DISCUSSION

Direct, flash schlieren, and time schlieren photographs of the combustion zone and flow field are the primary data of this study. Each method of observation produces a slightly different record of the experiment which must be interpreted with the technique used to obtain the record in mind. This section discusses the differences observed between various photographic techniques, indicates the reasons for selecting a particular observation technique, and presents the results obtained in this study with hydrogen-air mixtures. A procedure for computing an average flame-propagation velocity (derived in the appendix) is applied to the hydrogen flame angles of this study and the results of references 2 and 3.

Comparison of Photographic Techniques

Typical photographic results obtained by flash schlieren, direct, and time schlieren photographic techniques are shown in figure 2. All the photographs shown give the same

gross picture of the flame or reaction zone, that is, an approximately conical region starting at the tip of the nozzle centerbody with its axis coincident with the axis of the flow field.

Flash schlieren photographs.- Of the photographic techniques investigated in this study, the flash schlieren technique produces the most distinct record of a flame boundary in the flow field. Unfortunately, although figure 2(a) may be called typical in that respect, the regularity of the flame boundary is misleading. With approximately 10^{-6} second exposure, a flash schlieren photograph gives an essentially instantaneous record of the density gradients in the flow field and often shows large disturbances and asymmetry in the location of the flame boundary. Figure 3 gives an example of a flash schlieren in which one edge of the flame cone appears straight whereas the other has a large distortion including a portion where the flame boundary slopes toward the center line of the flow in the downstream direction. In order to establish an average representation of the flame boundary from flash schlieren photographs, a very large number of exposures of the same experimental conditions would be required. For this reason and because estimation of a straight flame surface from photographs like figure 3 is difficult to accomplish consistently, flash schlieren photographs were not used to determine average flame angle.

In an attempt to learn more about the behavior of the instantaneous schlieren flame boundary, several high-speed schlieren motion pictures of the flow field at different equivalence ratios were made. Individual frames of the films look very much like the single flash exposures in figure 2(a) and figure 3, although they are of poorer quality because of the additional optical components in the schlieren system and smaller image size necessary. Unfortunately, the maximum framing rate that could be achieved (about 1000 frames/second) was not sufficient to resolve the motion of the schlieren flame boundary. Consecutive frames show widely different positions and shapes of the flame boundary. When projected, the apparent motion of the flame boundary shown by the motion-picture film depends on the projection rate. However, it is clear from the motion-picture film that the disturbances in the instantaneous schlieren flame boundary increase in amplitude with increasing distance from the nozzle exit and mixture equivalence ratio. Also, because the motion of the disturbances could not be resolved, the rate at which the disturbances are generated must exceed 1000 per second.

Direct photographs.- Unlike the flash schlieren photographs, direct photographs of the flame like figure 2(b) represent a photographic averaging of the many flame positions and disturbances which occur during a relatively long exposure. Some difficulty was encountered in obtaining reasonably well exposed negatives over the range of equivalence ratio and, hence, for the flame luminosity studied. Initial attempts with a single exposure time and aperture (1/75 second and f2.5) were entirely inadequate. The addition of

variable aperture with a range from f2.5 to f16 did not help appreciably. Not only were negatives dim and underexposed below $\phi \approx 0.8$, but also pictures of approximately the same equivalence ratio showed $\pm 2^{\circ}$ or more scatter.

Adding exposure time as a variable, a number of direct photographs were obtained with a wide range of exposures at nearly constant equivalence ratio. Angles were measured from the negatives by approximating the upstream edges of the most exposed portion of the flame with lines drawn through the lip of the nozzle centerbody. Flame cone half-angle is taken as one-half the angle included between these lines. The flame angles measured from these photographs are shown in figure 4 plotted against relative exposure for $\phi \approx 0.6$, 0.8, and 1.0. Relative exposure (defined as exposure time divided by the square of the aperture) is proportional to the amount of light reaching the film plane for a subject of fixed brightness. As can be seen in figure 4, the measured flame angle increases with increasing relative exposure.

The effect of exposure on direct flame angle can be explained qualitatively with the help of the schlieren motion-picture results. Fluctuations in the schlieren flame boundary were noted which increase in magnitude with increasing distance along the flame from the nozzle exit. Thus, a long-time composite view of many flame positions and fluctuations like the direct photograph will show an increasing flame thickness with increasing distance along the flame. Varying exposures of the same flame would record a different angle for the flame edge because of the distribution of luminosity in the flame zone and the increase in apparent flame thickness with increasing distance from the nozzle exit.

In an attempt to eliminate or at least systematize the variation of apparent flame angle due to variation in exposure, an exposure schedule with equivalence ratio was established. A large number of negatives obtained with different exposures over a wide range of equivalence ratio were examined and a set of properly exposed negatives chosen. "Properly" exposed negatives were defined as those for which the region near the edges of the flame cone appeared to be more exposed than the region adjacent to the center line of the flow but did not quite saturate or fully expose the film. The direct photograph in figure 2(b) is printed from an underexposed negative (1/75-second exposure with $f = 5.6$) to accentuate this variation in luminosity through the flame cone. The logarithms of the relative exposures of these properly exposed negatives are plotted against equivalence ratio in figure 5, and as shown by the dashed line, a relatively good fit of the data is achieved with a straight line. It is interesting to note that an exposure variation of over three orders of magnitude is shown by the data. To the extent that the definition of proper exposure given represents uniform density of the film in the most exposed region of the flame, three orders of magnitude variation in exposure imply the same variation in flame luminosity.

An attempt was made to use the exposure schedule of figure 5 to obtain additional flame photographs for a wide range of equivalence ratio. However, since equivalence ratio could only be preselected with an accuracy of about ±0.1, most of the exposures obtained did not fall close to the exposure schedule. To systematize the effect of this exposure variation, a band including exposures a factor of two greater and less than the exposure schedule (that is, approximately one f stop overexposure and underexposure) was arbitrarily selected to represent proper exposure. This band lies between the solid lines in figure 5 labeled +1 and -1. Exposures outside the proper exposure band are classed as underexposed or overexposed. Most of these exposures fall within a factor of 4 or approximately two f stops of the boundaries of the proper exposure band as indicated by the lines labeled +3 and -3 in figure 5.

The flame angles measured from these negatives are shown plotted against equivalence ratio in figure 6 where the circular, square, and diamond symbols indicate proper, underexposure, and overexposure, respectively. Each plotted point represents the average of measurements made from at least six negatives comprising the sets of negatives obtained in several different runs. As expected, average angle increases with increasing exposure at all equivalence ratios, and the range of angles between underexposed and overexposed at $\phi \approx 1$ is more than 3°. Flame-angle data reported in reference 2, obtained under similar experimental conditions, are also shown in figure 6 by the triangular symbols. At low equivalence ratio these data lie below the underexposed data of the present study whereas at high equivalence ratio they lie above the overexposed data. Reference 2 does not specify whether a single exposure or an exposure variation was used in obtaining this data, and the number of measurements represented by each point is not given.

Time schlieren photographs.- From the discussion, it is apparent that substantial difficulty is involved in obtaining meaningful angle data from direct photographs. The large variation of flame luminosity with equivalence ratio requires a correspondingly large range of exposure to obtain photographs of comparable exposures at all equivalence ratios. Difficulty in predicting the equivalence ratio of a run gives rise to substantial variation in exposure from any desired schedule of exposure. Further, even with precise adherence to a schedule of exposure with varying equivalence ratio, the resulting flame-angle variation would depend on the particular schedule chosen.

In an attempt to find an observation technique without these shortcomings, a series of time-exposed schlieren photographs similar to the one shown in figure 2(c) were obtained. As in the direct photographs, a photographically averaged flame boundary is obtained with this technique because many flame positions and fluctuations occur during each exposure. But, since light is supplied from an external light source rather than from flame emission, no variation of exposure with equivalence ratio is required. The

circular symbols in figure 7 show flame angles measured from time schlieren negatives as a function of equivalence ratio. Underexposed direct flame-angle data from figure 6 are indicated for comparison. These sets of data produce essentially the same variation of angle with equivalence ratio from $\phi \approx 0.2$, where a propagating flame is first observed in direct photographs, to the highest equivalence ratio for which data were obtained.

The close correspondence of the underexposed direct and time schlieren flame angles provides a meaningful physical interpretation of the location of the time schlieren boundary in the flame front. In direct photographs at a given equivalence ratio, the measured flame angle decreases with decreasing exposure until the flame intensity is not sufficient to expose the negative, and flame angle can no longer be measured. With decreasing exposure from overexposed to underexposed, the direct flame angle can be thought of as representing first the locus of maximum advance of the flame and finally the locus of maximum luninosity within the flame. Since the time schlieren flame angles lie close to the underexposed direct photograph results, the time schlieren flame boundary can be interpreted as representing the locus of maximum luminosity within the flame.

Flame-Angle Data

Because the time schlieren flame boundary appears to correspond to the locus of maximum luminosity within the flame and because the time schlieren technique proved to be far simpler and more reliable than the direct photograph method, time schlieren photographs were used as the recording technique for flame observation throughout the remainder of the study. It was found that measurement scatter could be reduced by orienting the schlieren knife edge perpendicular to the center line of the flow. With this knife-edge orientation, the schlieren image appears to be symmetrical about the center line of the flow, and no consistent difference in flame boundary angle to either side of the center line could be detected. Generally speaking, scatter in multiple measurements from a single negative is less than $\pm 0.5^{\circ}$. Several photographs of the same run or different runs at the same equivalence ratio showed an angle variation less than $\pm 1^{\circ}$. With the time schlieren technique, as many as five photographs could be obtained in a single 10-second run, and a large number of runs over the range of equivalence ratio studied were accomplished. Thus, the flame-angle data presented are the averages of measurements from many photographs obtained in several runs.

Figure 8 presents the variation in average flame angle with equivalence ratio obtained in this study by using the time schlieren technique. Data for initial mixture stagnation temperature of 300° K from figure 7 and additional data for 450° K are shown. For both mixture temperatures, the flame angle is approximately 2° at $\phi = 0.2$ and increases rapidly with equivalence ratio to $\phi \approx 0.8$. For $\phi > 0.8$, the flame angle remains approximately constant and independent of equivalence ratio. With a stagnation

temperature of 300° K, the flame angle for a stoichiometric mixture is approximately 9.2°. Increasing the stagnation temperature to 450° K decreases the flame angle measured for a stoichiometric mixture to about 7.4°.

The horizontal line at $\phi \approx 0.1$ indicates the schlieren boundary angle for mixing between the pilot jet and air. No change in the boundary angle could be detected at the different stagnation temperatures. An increase in the boundary angle is noted at $\phi \approx 0.2$ which corresponds roughly to the equivalence ratio for which a flame that appears to propagate is first observed visually or in direct photographs. It should be noted that the lower limit of propagation could not be well defined. The hot pilot gas could certainly initiate chemical reaction in a mixture too lean to support flame propagation, and the length of flow field observed was not sufficient to determine whether a flame was propagating at small boundary angles.

Flame-Propagation Velocity

The concept of a flame-propagation velocity has proved a useful one in the study of laminar flames. Flame-propagation velocity is defined as the component of flow velocity in the unburned gas perpendicular to the flame surface, and often, an average value for an entire flame is determined from experimentally observed flame shape and some knowledge of the experimental flow field. Various authors have extended the concept of flame-propagation velocity to turbulent flows. (Ref. 4 contains a recent review of the literature of laminar and turbulent flame propagation.) Definition of a representative flame surface becomes more difficult in turbulent flow, and somewhat arbitrary methods of defining an average flame surface must be adopted that suit the geometry of the particular experiment.

Earlier work reported in references 1 and 3 with an experimental configuration similar to that used in the present study presented burning velocity computed from the relation:

$$u_F \equiv V_0 \sin \theta \tag{1}$$

This relation yields flame-propagation velocity based on the assumption that the velocity of the unburned gas ahead of the flame front is equal to the free-stream velocity and parallel to the center line of the flow. As shown in the appendix, this assumption is equivalent to requiring that

$$\rho_u V_u = \rho_b V_b \tag{2}$$

This relation implies a substantial decrease in static pressure across the flame because of the large flow velocities in the present experiments. Measurements reported in reference 1 indicate no large static-pressure variation in the flame region; thus, some deflection of the flow ahead of the flame may be expected.

An analysis to determine the flame-propagation velocity without assuming the flow ahead of the flame to be parallel to the center line is presented in the appendix. The expression derived for the component of velocity normal to the experimentally observed flame surface can be written

$$v_n = \frac{\rho_b}{\rho_u} V_b \sin \theta \tag{3}$$

where the subscript u denotes unburned gas immediately upstream of the flame and the subscript b denotes burned gas downstream of the flame where the velocity is assumed to be parallel to the center line of the flow. Propagation velocity can be computed from this expression if measurements in or assumptions concerning the flow field are made to allow computation of the density ratio across the flame and the velocity of the burned gas.

In the appendix two simple flow process assumptions are considered which bound the experimental situation. In the first process, any turning of the flow upstream of the flame is assumed to occur without an increase in static pressure as suggested by the measurements reported in reference 1. Because this assumption leads to the computation of substantial flow turning angles ahead of the flame, the effect of an increase in static pressure accompanying turning ahead of the flame should also be considered. Thus, in the second flow process, the static pressure ahead of the flame is assumed to increase with turning by an amount corresponding to a specified fraction η of the pressure rise for an isentropic two-dimensional turn. Since the experimental flow field is axisymmetric, the range of pressures between constant static pressure ($\eta = 0$) and the pressure for an isentropic two-dimensional turn ($\eta = 1$) should include conditions equivalent to the experimental flow field.

Flame-propagation velocity computed with the average flame angles of figure 8 for 300° K and 450° K mixture temperatures and the assumption of constant pressure turning ahead of the flame are shown in figure 9. The computed flame-propagation velocities, much like the flame-angle data, increase rapidly with equivalence ratio to a value which remains approximately constant for $\phi > 0.8$. Unlike the flame angle which decreases with increasing mixture stagnation temperature, the computed flame propagation velocity increases almost 50 percent when the mixture stagnation temperature is increased from 300° K to 450° K. This increase in flame-propagation velocity is easily explained in qualitative terms by inspection of equation (3). Propagation velocity is proportional to density ratio ρ_b/ρ_u across the flame. The unburned density decreases inversely with

the mixture stagnation temperature (if fixed Mach number, equivalence ratio, and static pressure are assumed), but the burned density is almost independent of small changes in unburned density for fixed static pressure. Burned gas velocity is likely to increase since nozzle exit velocity increases while the measured flame angle decreases. Thus, the effects of changing stagnation temperature on burned gas velocity and flame angle are opposite. The principal effect of changing stagnation temperature is to change the density ratio across the flame front, and flame-propagation velocity may be expected to increase approximately proportional to stagnation temperature.

If some rise in static pressure is associated with the turning ahead of the flame, generally higher flame-propagation velocities are computed. At low equivalence ratio, where flame angle and flow deflection are small, only a small pressure rise and increase in propagation velocity occur even with isentropic two-dimensional compression. At a higher equivalence ratio, substantial turning ahead of the flame can produce significant increases in static pressure and corresponding changes in computed flame-propagation velocity. Figure 10 demonstrates the magnitude of the effect of pressure rise for flame angles typical of $\phi \approx 1$ with mixture temperatures of 300° K and 450° K. With 300° K mixture stagnation temperature, a 40-percent increase in flame-propagation velocity is computed if isentropic two-dimensional compression ahead of the flame is assumed ($\eta = 1.0$); for 450° K an increase of 20 percent is computed. Although the appropriate value of η or the variation of η with equivalence ratio is not known, it is interesting that the slope of the curve for the velocity plotted against η is greatest near $\eta = 0$. Thus, even if only one-third of the two-dimensional compression static-pressure rise is achieved ($\eta \approx 0.3$), propagation velocity increases of 20 percent and 10 percent are computed for 300° K and 450° K mixture temperatures, respectively. Although these propagation velocity increases are significant, it should be noted that even with $\eta = 1$, substantial turning angles ahead of the flame are computed, and the flame-propagation velocities are not nearly as large as values of u_F computed from equation (1). The flame angles used in computing figure 10 and the resulting flow deflections, static pressures, and so forth, are listed in table I.

Although the experiments of the present study are restricted to hydrogen fuel, flame-angle data for several hydrocarbon fuels are available in reference 3. Flame-propagation velocities computed from these data by the technique described in the appendix are shown in figure 11. No common trend of propagation velocity with equivalence ratio is apparent. The flame-propagation velocity for methane decreases continuously with increasing equivalence ratio whereas for ethane and ethylene, computed propagation velocity is approximately constant and independent of equivalence ratio.

Figure 11 does indicate a definite distinction in flame-propagation velocity between hydrogen and the different hydrocarbon fuels. It is interesting to note that the order and

TABLE I.- REPRESENTATIVE FLAME ANGLES AND COMPUTED RESULTS FOR STOICHIOMETRIC HYDROGEN-AIR MIXTURES

Nozzle exit velocity, m/sec	501	501	614	614
Stagnation temperature, °K	300	300	450	450
θ, deg	9.10	9.10	7.25	7.25
α, deg	8.14	7.58	6.15	5.79
p_1, atm	1.0	1.37	1.0	1.28
v_n, m/sec	8.40	11.75	11.77	14.23
Flow-process assumption	Constant pressure	2-dimensional compression	Constant pressure	2-dimensional compression

relative magnitude of the hydrocarbon flame-propagation velocities presented in figure 11 are similar to the behavior of laminar burning velocities. As shown in table II, maximum laminar burning velocities from reference 5 for ethane and ethylene are 1.2 and 2.0 times the maximum laminar burning velocity for methane. The computed flame-propagation velocities for ethane and ethylene at $\phi = 1.0$ shown in figure 11 are 1.4 and 2.5 times the value for methane. Also as indicated in table II, for stoichiometric hydrogen-air mixtures the laminar burning velocity from reference 6 is 5.6 times the maximum value for methane. In figure 11 at $\phi = 1.0$, the computed flame-propagation velocity for hydrogen is 3.2 times the value for methane.

Even such qualitative similarity as that shown in table II between laminar burning velocities and the computed flame-propagation velocities of this study is surprising. The experimental flow of the present study is vastly different from the type of experiment used to determine laminar burning velocity. A shortcoming of the comparison in table II

TABLE II.- COMPARISON OF FLAME-PROPAGATION VELOCITIES OF PRESENT STUDY WITH LAMINAR BURNING VELOCITIES

Fuel	Flame-propagation velocity			
	Laminar values		Present study (fig. 11)	
	m/sec	Relative to methane	m/sec	Relative to methane
Methane	[a]0.34	1.0	2.6	1.0
Ethane	[a].40	1.2	3.7	1.4
Ethylene	[a].68	2.0	6.4	2.5
Hydrogen	[b]1.90	5.6	8.4	3.2

[a]Maximum laminar values from reference 5.

[b]Stoichiometric value from reference 6.

may be found in the temperature level of the laminar data. This laminar data corresponds to mixtures at about 300° K whereas in the present study a mixture stagnation temperature of 300° K corresponds roughly to a static temperature ahead of the flame of 210° K. Sufficient information to estimate laminar burning velocities at 210° K could not be found in the literature. However, since the important comparison in table II is between values relative to methane in each apparatus, the difference in initial temperature should not change the qualitative result shown.

Additional flame-angle data are presented in reference 3 for hydrogen, ethane, and ethylene mixtures at stagnation temperatures above 300° K. Flame-propagation velocities computed from these data are shown plotted against mixture static temperature in figure 12 along with values computed for the hydrogen data of this study. The ethane data from reference 3 show an approximately linear increase of the logarithm of flame-propagation velocity with increasing mixture static temperature from 210° K to 500° K. Reference 3 presents hydrogen and ethylene data for static temperatures of 210° K and 360° K. As can be seen in figure 12, the slope of a line through each pair of points is approximately the same as the trend of the ethane data. Hydrogen data from the present study agree closely with the data from reference 3 at 210° K. However, the increase of propagation velocity with an increase in static temperature to 320° K shown by the data of the present study is far less than expected from the data of reference 3.

The explanation of this difference between the results of reference 3 and the present study is not known. It is possible that the variation of the logarithm of flame-propagation velocity with mixture static temperature is not smooth or perhaps that the variations for hydrogen and ethane are not alike. Also, the data in reference 3 were obtained with hydrogen-vitiated air (air heated by mixing with hydrogen-oxygen combustion products) whereas the present study is based on data with clean air. Differences in flame-observation techniques also exist, but since the data of reference 3 and the present study agree at 210° K static temperature for $\phi = 0.65$, the techniques appear to be equivalent. In the present study, changes in mixture temperature were not found to affect the exposure required for direct photographs.

CONCLUDING REMARKS

Time-exposed schlieren photographs provide a simple method for obtaining a reproducible, average record of flame position. Comparison with direct photographs of varying exposure indicates that the flame boundary apparent in time schlieren photographs corresponds to the locus of maximum luminosity within the flame. Flame cone half-angles measured from time schlieren photographs are found to increase rapidly with equivalence ratio from 2° at an equivalence ratio of approximately 0.2 up to an equivalence

ratio of approximately 0.8 and remain approximately constant at higher equivalence ratio. For stoichiometric mixtures, flame angle is approximately 9.2° for a stagnation temperature of 300° K; increasing the stagnation temperature to 450° K decreases the flame angle to about 7.4°. Flame-propagation velocity computed from time schlieren flame angles is found to vary with equivalence ratio in the same manner as flame angle. However, increasing the mixture stagnation temperature from 300° K to 450° K increases the computed flame-propagation velocity. Relative values of flame-propagation velocity for hydrogen, methane, ethane, and ethlyene computed from flame angles of the present study and data from similar experiments reported in reference 3 were found to be similar to laminar burning velocities. The trend of flame angle with stagnation temperature for mixtures of hydrogen and air found in the present study is substantially different from the trend expected based on the data of AIAA paper 66-573.

Langley Research Center,
National Aeronautics and Space Administration,
Langley Station, Hampton, Va., April 16, 1968,
126-15-03-20-23.

APPENDIX

FLAME-PROPAGATION VELOCITY

The flame-propagation velocity presented in the body of this report, defined as the component of mean flow velocity perpendicular to the average flame surface location, was computed from the experimental data by using the relations derived below. The flame is assumed to be approximately conical with a half-angle θ as shown in sketch (a).

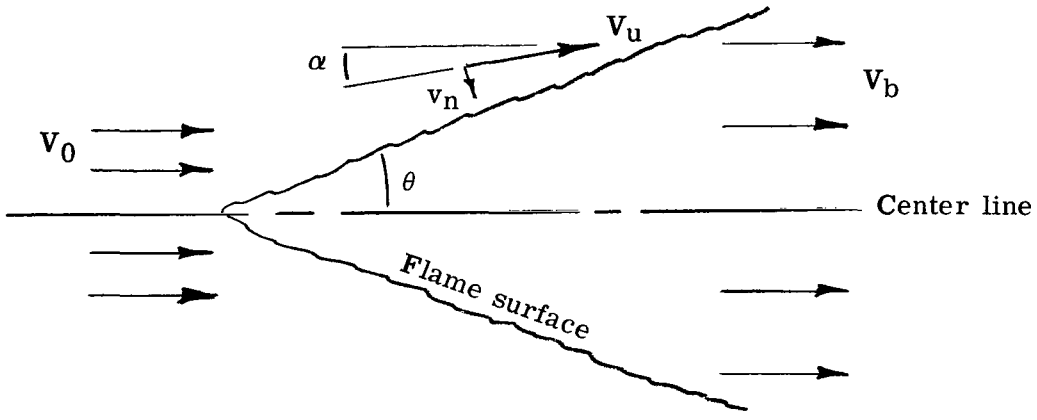

Sketch (a)

The flow leaving the nozzle, denoted by the subscript 0, has a velocity V_0 and is assumed to be uniform and parallel. Flow upstream of the flame, denoted by the subscript u, has a velocity V_u at some angle α with the center line of the flow. Flow downstream of the flame, denoted by subscript b, has velocity V_b which is assumed to be parallel to the center line of the flow. The conservation of mass applied to a small element of flame surface gives

$$\rho_u V_u \sin(\theta - \alpha) = \rho_b V_b \sin \theta \tag{A1}$$

at any position along the flame. The component of velocity normal to the flame surface or propagation velocity can be written as

$$v_n = V_u \sin(\theta - \alpha) \tag{A2}$$

If, as in references 1 and 3, the velocity ahead of the flame is assumed to be parallel to the center line of the flow ($\alpha = 0$) and equal to the nozzle exit velocity, equation (A1) gives

$$v_n = V_0 \sin \theta \tag{A3}$$

Equation (A3) is equivalent to the expression used to compute burning velocity in references 1 and 3. It should be noted that if $\alpha = 0$, equation (A1) reduces to

$$\rho_u V_u = \rho_b V_b \tag{A4}$$

Since a large decrease in density is expected in the flame, equation (A4) implies that a large increase in velocity must occur if $\alpha = 0$ is a valid approximation. Since the unburned gas velocity is large, a large increase in velocity across the flame implies a substantial decrease in static pressure in order to satisfy the conservation of momentum. However, the experiments were conducted in a low supersonic Mach number, free-jet configuration adjusted to match atmospheric pressure, and large variations in static pressure are not expected. Also, the experimental measurements reported in reference 1 for a similar configuration show variations in static pressure of only ±1 pound per square inch (6.89×10^3 newtons per meter^2) through the flame zone and along the jet center line within 15 centimeters of the nozzle exit.

Thus, assuming $\alpha = 0$ does not appear to be reasonable since this assumption implies large variations in static pressure across the flame which are not expected in the experimental configuration and were not found in the measurements reported in reference 1. Rearranging equation (A1) and substituting the result into equation (A2) yields

$$v_n = \frac{\rho_b}{\rho_u} V_b \sin \theta \tag{A5}$$

By using this expression, flame-propagation velocity can be evaluated from the measured flame angle if the ratio of burned gas to unburned gas density and the burned gas velocity are known. Two simple flow processes which provide a means for computing these quantities and allow evaluation of the flame-propagation velocity from equation (A5) are discussed.

The first flow process relies on the assumption that the static pressure is constant throughout the flow field from the nozzle exit plane to the region downstream of the flame as suggested by the static-pressure measurements reported in reference 1. Because this flow process leads to the computation of substantial turning in the supersonic flow ahead of the flame, a second process is defined in which the static pressure ahead of the flame is increased with turning by an arbitrary fraction of the pressure rise for isentropic, two-dimensional turning. Since the experimental flow field is axisymmetric, the static pressure ahead of the flame probably falls between the values computed with these two flow process assumptions. The intent of the analysis is limited to providing

estimates of flame-propagation velocity which are likely to bound the actual propagation velocity in the experiment.

Constant Pressure

If the entire flow field is assumed to be at the same static pressure as the nozzle exit plane, then for momentum to be conserved the fluid velocity must be constant throughout the flow field.

$$V_u = V_b = V_0 \tag{A6}$$

From the equation of state for a perfect gas, the density ratio across the flame, if constant pressure is assumed, can be written

$$\frac{\rho_b}{\rho_u} = \frac{\mathcal{M}_b}{\mathcal{M}_u}\frac{T_u}{T_b} \tag{A7}$$

The combustion process for hydrogen-air mixtures, complete combustion and no dissociation being assumed, can be represented by the reaction:

$$(3.77N_2 + O_2) + 2\phi H_2 \rightarrow 3.77N_2 + (1 - n)\left[2\phi H_2O + (1 - \phi)O_2\right] + 2n\left[H_2O + (\phi - 1)H_2\right] \tag{A8}$$

where ϕ is the equivalence ratio, and the index $n = 0$ for $\phi \leqq 1$ and $n = 1$ for $\phi > 1$. From this reaction the ratio of burned gas molecular weight to unburned gas molecular weight becomes

$$\frac{\mathcal{M}_b}{\mathcal{M}_u} = \frac{4.77 + 2\phi}{(4.77 - n) + (1 + n)\phi} \tag{A9}$$

With the assumption of constant static pressure and hence velocity across the flame, the kinetic energy of the fluid remains constant, and the conservation of energy requires that any heat released in the chemical reaction appear as sensible energy by an increase in fluid static temperature. This flow process is equivalent to constant pressure combustion of the fluid at rest; and, hence, the ratio of unburned gas static temperature to burned gas static temperature can be written as

$$\frac{T_u}{T_b} = \frac{T_0}{T_0 + \Delta T_c} \tag{A10}$$

where ΔT_c is the temperature rise for constant-pressure combustion of the fuel-air mixture at rest. A schedule of combustion temperature rise with equivalence ratio for an initial static temperature typical of the nozzle exit static temperature range in the present experiments was taken from the real-gas equilibrium computations presented in reference 7. Thus, with the assumption of constant static pressure throughout the flow field, the expression for flame-propagation velocity becomes

$$v_n = \left[\frac{4.77 + 2\phi}{(4.77 - n) + (1 + n)\phi}\right] \frac{T_0}{T_0 + \Delta T_c} V_0 \sin \theta \tag{A11}$$

In calculating flame-propagation velocity from the hydrocarbon flame angles of reference 3, the molecular weight change in combustion was neglected. Also, the combustion temperature rise was assumed to be proportional to equivalence ratio for $\phi \leq 1$ and constant for $\phi > 1$ as follows:

$$\Delta T_c = \left[n + (1 - n)\phi\right] \Delta T_c \Big]_{\phi=1} \tag{A12}$$

Values of combustion temperature rise for stoichiometric mixtures were taken from reference 5. Since for constant static pressure throughout the flow field, $V_b = V_0$, flame-propagation velocity for the hydrocarbon fuel data of reference 3 becomes

$$v_n = \frac{T_0 V_0 \sin \theta}{T_0 + \left[n + (1 - n)\phi\right] \Delta T_c \Big]_{\phi=1}} \tag{A13}$$

Two-Dimensional Compression

In the preceding section, relations are derived to compute flame-propagation velocity from experimental flame-angle data based on the assumption that the entire flow is at constant static pressure. The flow model considered presumes that the flow between the nozzle exit plane and the flame is turned away from the center line without a significant increase in static pressure. Since the flow is supersonic, this assumption is, at best, an approximation restricted to small amounts of turning. Therefore, it is of interest to use the assumption of constant-pressure turning to estimate the amount of turning ahead of the flame. If this turning is not small, modification of the constant-pressure assumption may be required.

Equation (A1) can be rearranged to give the deflection ahead of the flame as follows:

APPENDIX

$$\alpha = \theta - \sin^{-1}\left(\frac{\rho_b V_b}{\rho_u V_u} \sin \theta\right) \tag{A14}$$

As before, if the static pressure throughout the flow field is assumed to be constant, then from the conservation of momentum $V_b/V_u = 1$. Substituting values for a stoichiometric mixture of hydrogen and air in equations (A9) and (A10), the density ratio can be determined from equation (A7) as $\rho_b/\rho_u \approx 0.1$. Thus, if the deflection of the flow ahead of the flame is assumed to occur at constant pressure, equation (A6) leads to $\alpha \approx 0.9\theta$ for a stoichiometric mixture of hydrogen and air. Since the flow ahead of the flame is supersonic, some increase in static pressure is likely to occur for such substantial turning, and the assumption of constant static pressure may be misleading.

To check the magnitude of the increase in static pressure due to turning ahead of the flame and the effect of this pressure rise on the computed flame-propagation velocity, the analysis described in the preceding section was modified to include an increase of static pressure upstream of the flame dependent on turning. The flow between the nozzle exit plane and the upstream edge of the flame is assumed to contain a series of compression waves which increase the static pressure from the nozzle exit value. The static pressure upstream of the flame is increased by an arbitrary specified fraction of the static-pressure rise resulting from a two-dimensional, isentropic turn to the flow direction upstream of the flame. For a two-dimensional isentropic turn, the local pressure coefficient is given by (see eqs. 10.22 and 14.11 of ref. 8)

$$c_p \equiv \frac{p - p_0}{\frac{1}{2}\rho_0 V_0^2} \approx \frac{2}{\sqrt{M_0^2 - 1}}\left(\frac{dy}{dx}\right)_{\text{Streamline}} \tag{A15}$$

By using the equation of state, the definition of Mach number for a perfect gas, and equation (A15), the static pressure upstream of the flame can be written

$$p_1 = p_0\left(1 + \eta \frac{\gamma M_0^2}{\sqrt{M_0^2 - 1}} \tan \alpha\right) \tag{A16}$$

The factor η is included in equation (A16) to provide a convenient means for varying the static pressure assumed upstream of the flame. Note that for $\eta = 0$, equation (A16) reduces to $p_1 = p_0$ and is equivalent to the assumption of turning at constant static pressure. Since the experimental flow field is axisymmetric, the range of pressures between constant pressure ($\eta = 0$) and isentropic, two-dimensional compression ($\eta = 1$)

should include conditions ahead of the flame equivalent to those in the experimental flow field. Since the combustion products downstream of the flame are subsonic, this increased static pressure is not expected to persist, and an isentropic expansion process was arbitrarily selected to reduce the static pressure downstream of the flame to the nozzle exit value.

With these assumptions an iterative computation of flame-propagation velocity can be performed. From nozzle exit conditions at 0 where the flow is assumed uniform and parallel, a trial value of α is assumed. (See sketch (b).) The static pressure

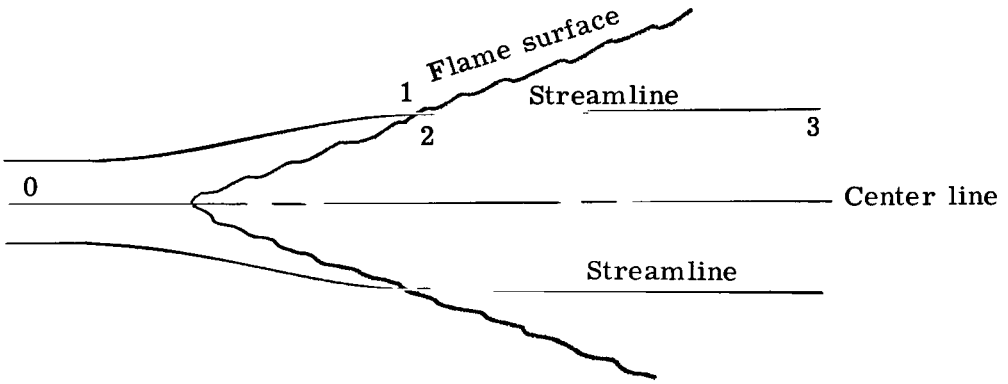

Sketch (b)

immediately upstream of the flame surface at station 1 is computed from equation (A16) with a particular value of η. Other properties upstream of the flame are computed from the static pressure with conventional relations for the one-dimensional isentropic flow of a perfect gas. The conditions immediately downstream of the flame are then computed by reacting the flow at constant pressure by using the relations employed in the previous section, namely, equations (A9) and (A10). The combustion products are then expanded (stations 2 to 3) to the nozzle exit plane static pressure by using conventional relations for the one-dimensional isentropic flow of a perfect gas. A new value of α is calculated from equation (A14) with the unburned conditions taken as the values computed at station 1 and the burned-gas conditions taken as those computed at station 3. This new α is used to start the computations at station 1 again. The calculations are continued until successive values of α are within a specified tolerance. This procedure was programed for a digital computer and used for all burning velocity computations presented in this report.

REFERENCES

1. Slutsky, S.; Tamagno, J.; and Trentacoste, N.: An Experimental and Analytical Investigation of Ignition and Axisymmetric Turbulent Flame Propagation in Premixed Hydrogen-Air Flows With Application to Supersonic Combustion. AIAA Paper No. 65-40, Jan. 1965.

2. Slutsky, S.; Tamagno, J.; and Trentacoste, N.: Supersonic Combustion in Premixed Hydrogen-Air Flows. AIAA J., vol. 3, no. 9, Sept. 1965, pp. 1599-1605.

3. Slutsky, S.; Tamagno, J.; and Fruchtman, I.: An Analysis of Hydrocarbon-Air Combustion Flames. AIAA Paper No. 66-573, June 1966.

4. Williams, Forman A.: Combustion Theory. Addison-Wesley Pub. Co., Inc., c.1965.

5. Propulsion Chemistry Division, Lewis Flight Propulsion Laboratory: Basic Considerations in the Combustion of Hydrocarbon Fuels With Air. NACA Rep. 1300, 1957.

6. Heimel, Sheldon: Effect of Initial Mixture-Temperature on Burning Velocity of Hydrogen-Air Mixtures With Preheating and Simulated Preburning. NACA TN 4156, 1957.

7. Drell, Isadore L.; and Belles, Frank E.: Survey of Hydrogen Combustion Properties. NACA Rep. 1383, 1958. (Supersedes NACA RM E57D24.)

8. Shapiro, A. H.: The Dynamics and Thermodynamics of Compressible Fluid Flow. Vol. I. The Ronald Press Co., c.1953.

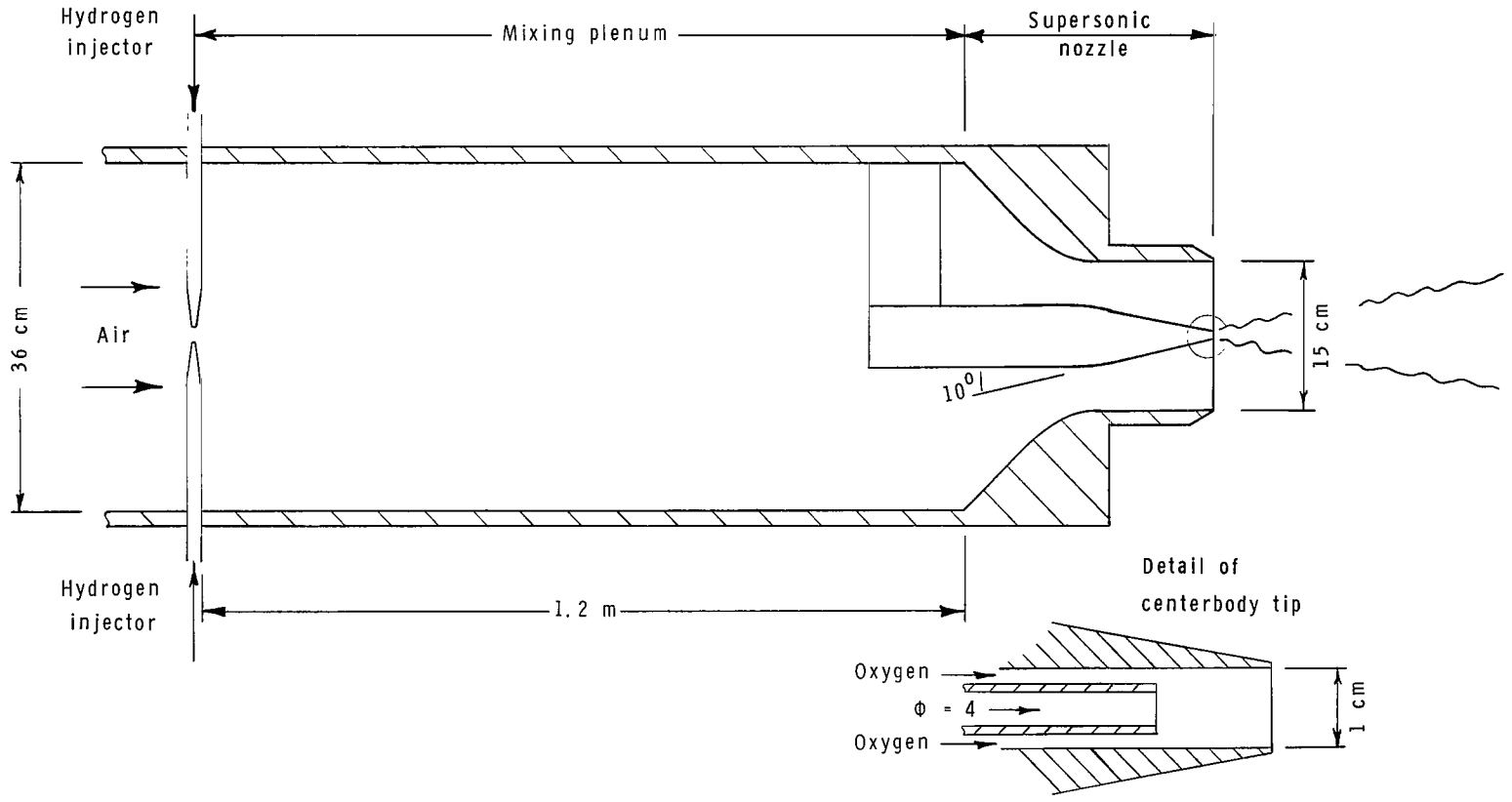

Figure 1.- Apparatus schematic.

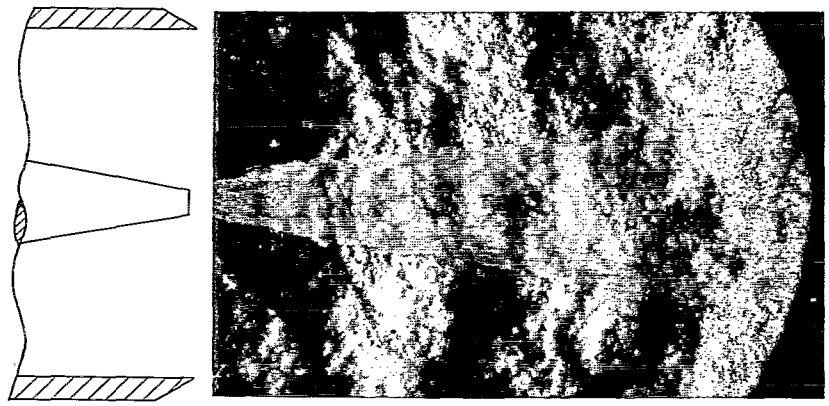

(a) Flash schlieren.

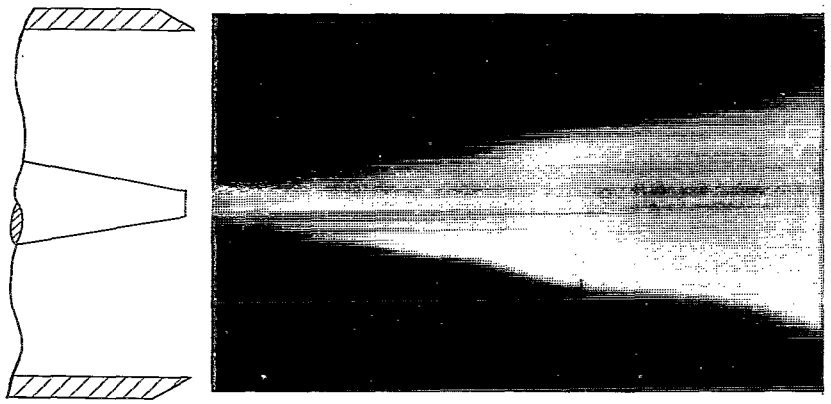

(b) Direct.

(c) Time schlieren. L-68-877

Figure 2.- Typical flash schlieren, direct, and time schlieren photograph results. Stoichiometric hydrogen and air with stagnation temperature of 300° K.

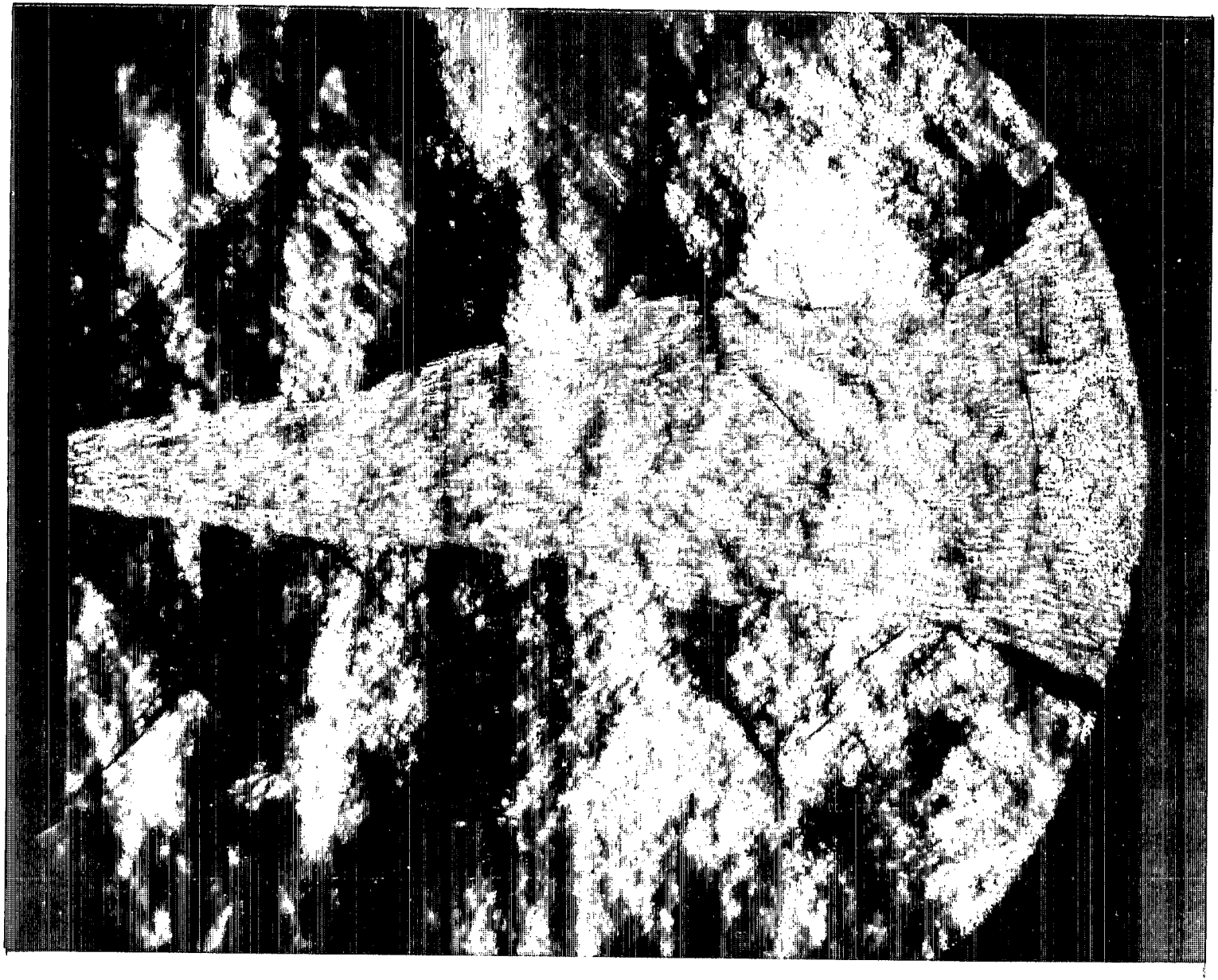

Figure 3.- Asymmetric flash schlieren photograph. L-68-878

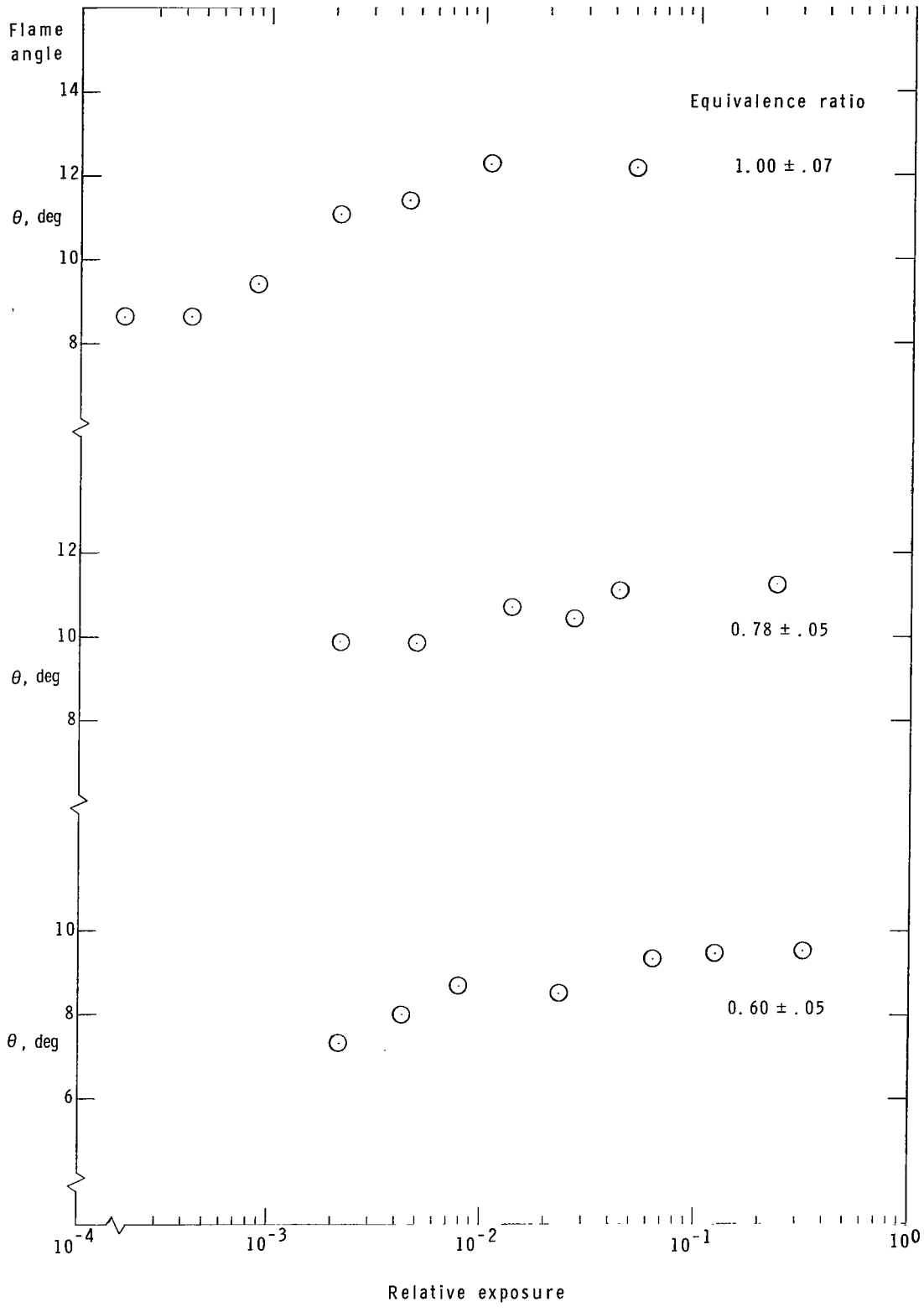

Figure 4.- Flame angle from direct photographs plotted against relative exposure.

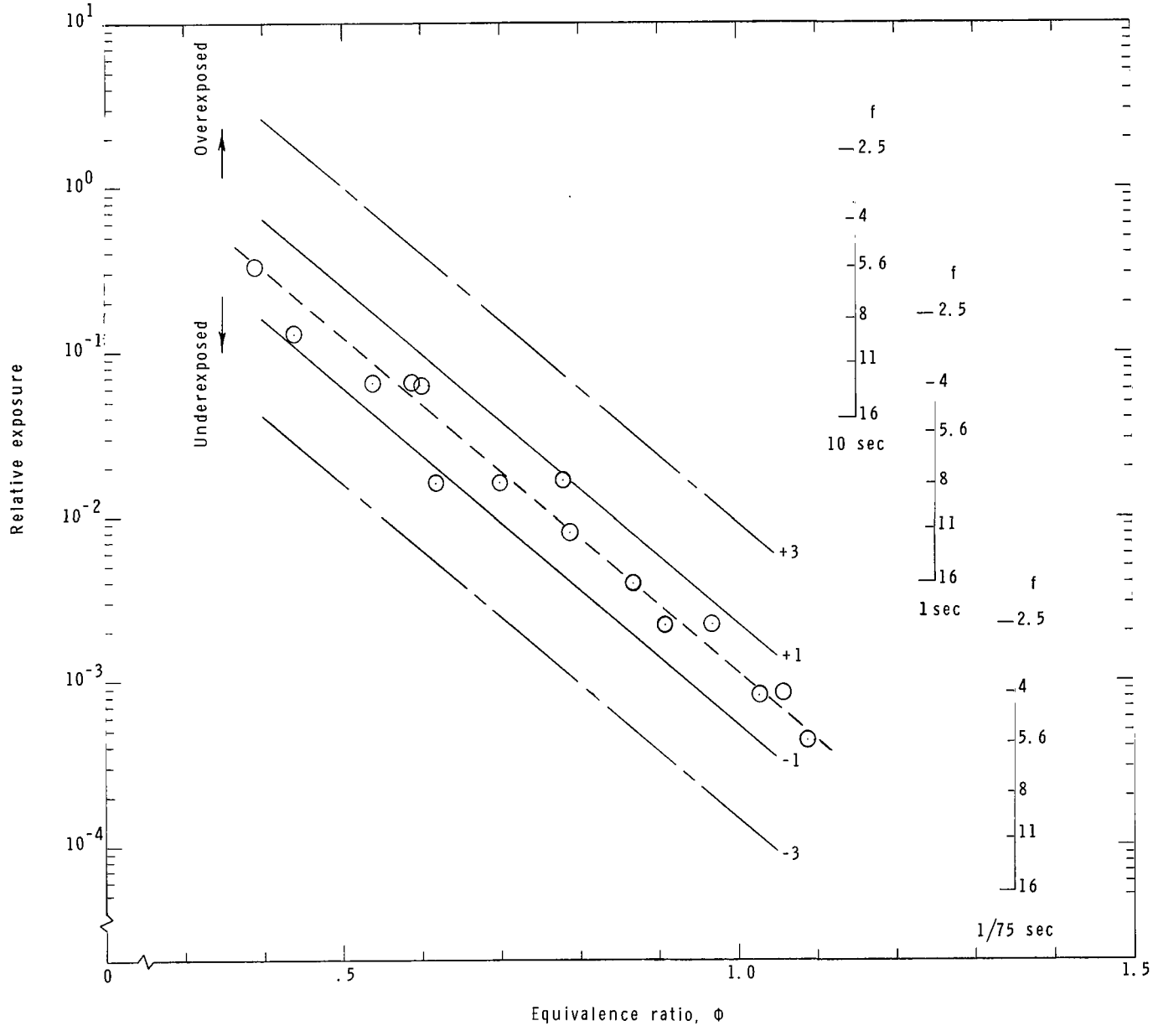

Figure 5.- Direct photograph exposure schedule.

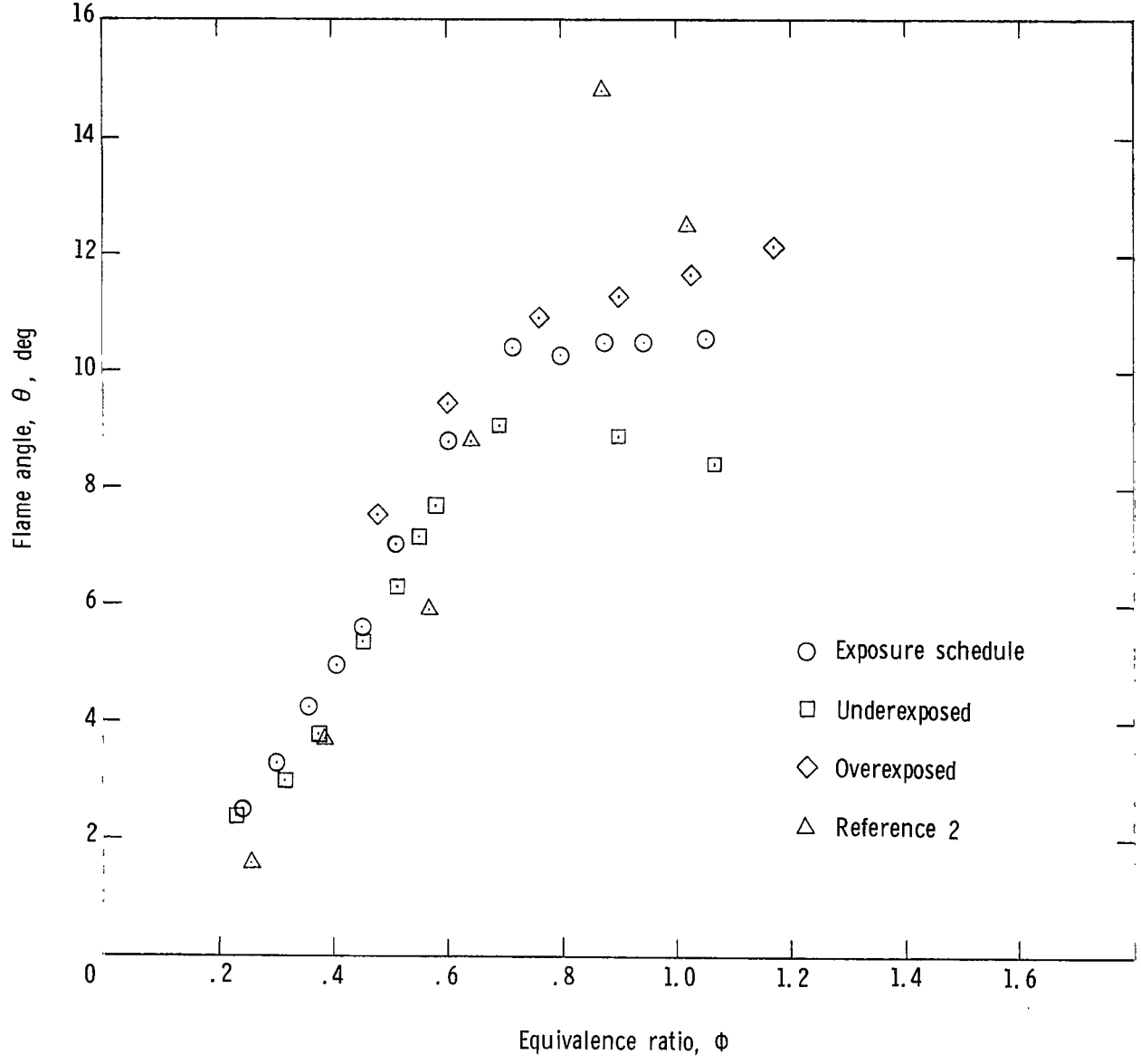

Figure 6.- Flame angle from direct photographs plotted against mixture equivalence ratio. Stagnation temperature, 300° K.

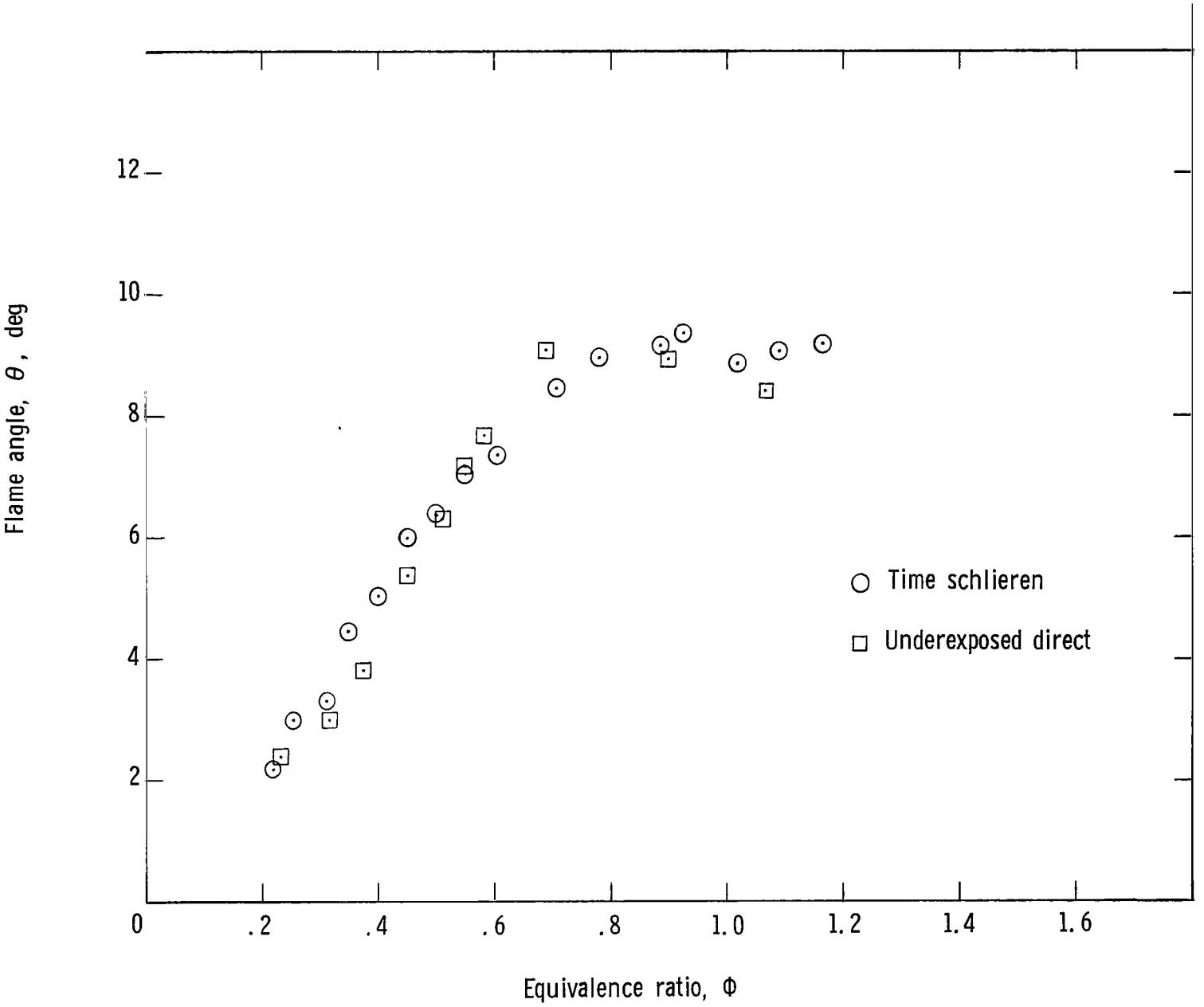

Figure 7.- Time schlieren and underexposed direct flame angles plotted against equivalence ratio. Stagnation temperature, 300° K.

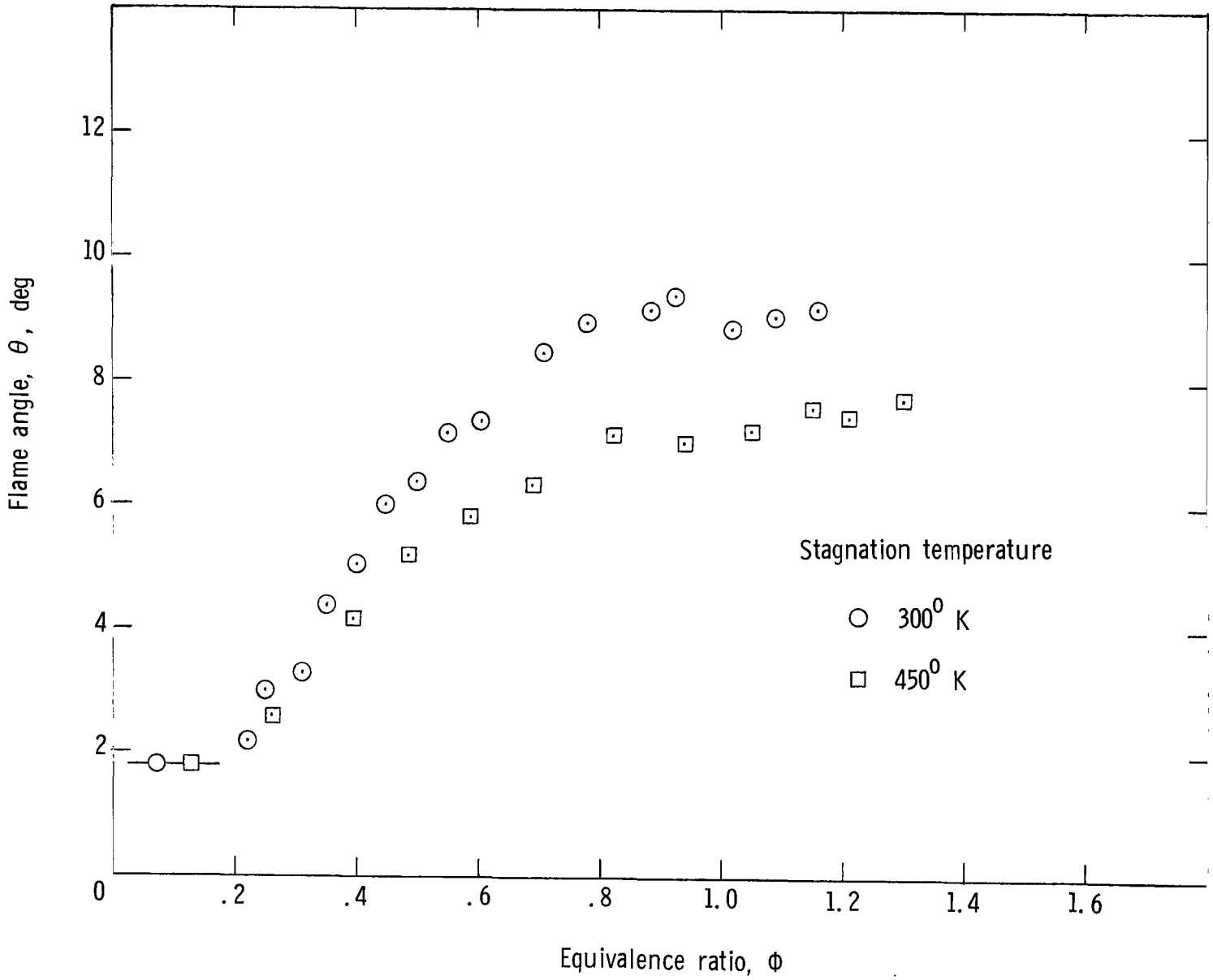

Figure 8.- Time schlieren flame angle plotted against equivalence ratio for mixture temperatures of 300° K and 450° K.

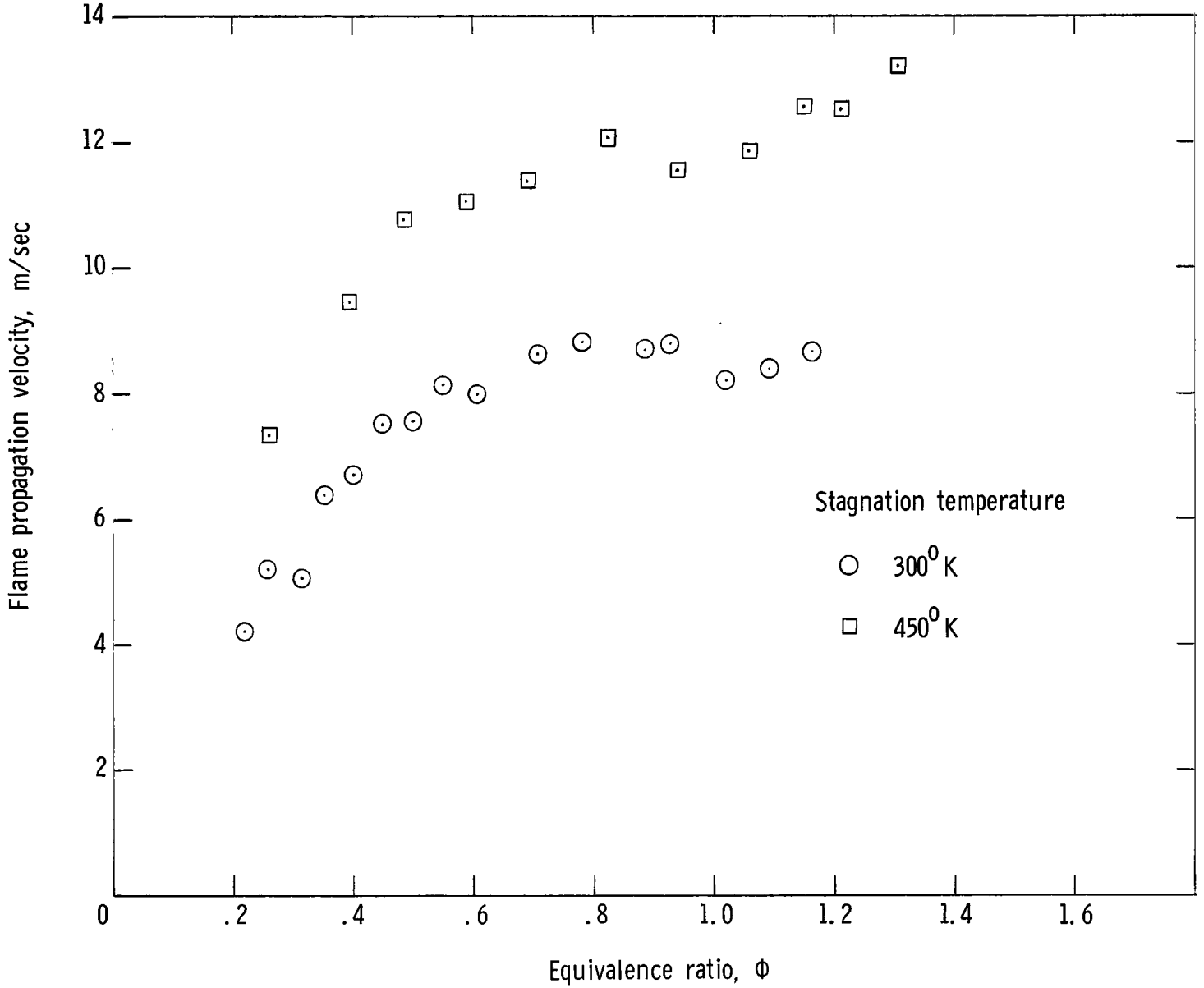

Figure 9.- Flame propagation velocity plotted against equivalence ratio for hydrogen-air mixture. Constant pressure.

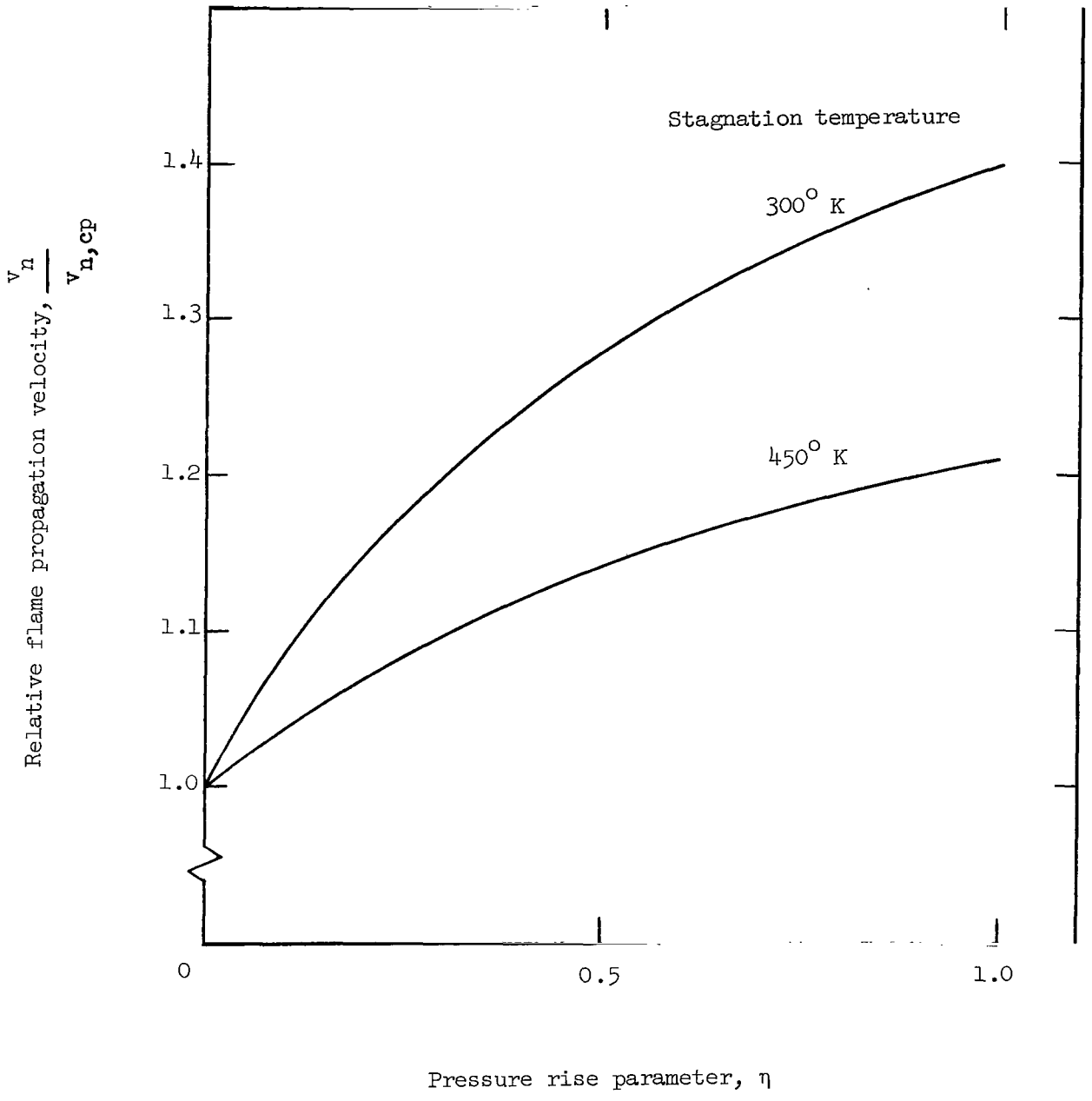

Figure 10.- Relative flame propagation velocity plotted against pressure rise parameter.

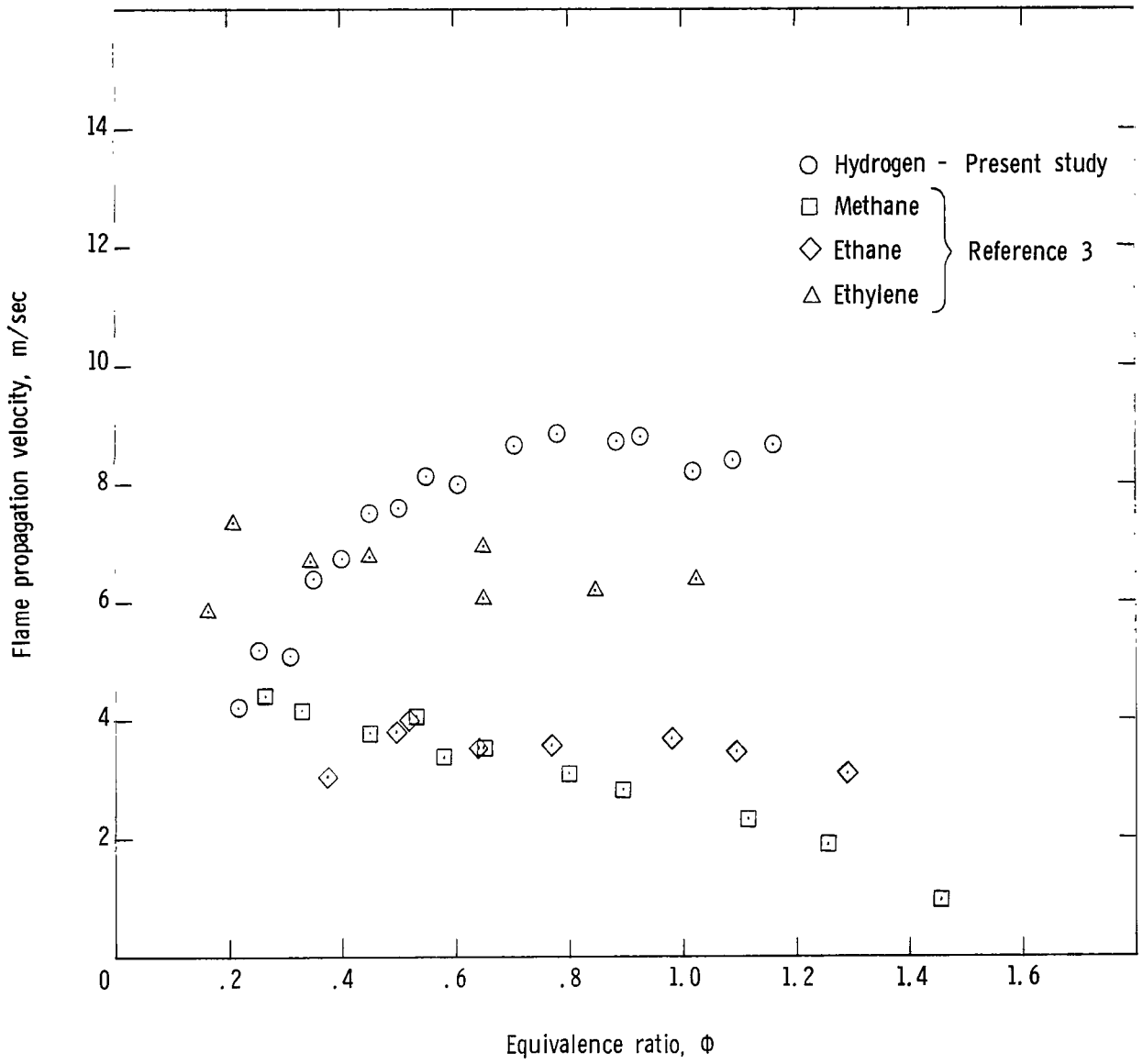

Figure 11.- Flame propagation velocity plotted against equivalence ratio for hydrogen, methane, ethane, and ethylene. Stagnation temperature, 300^0 K.

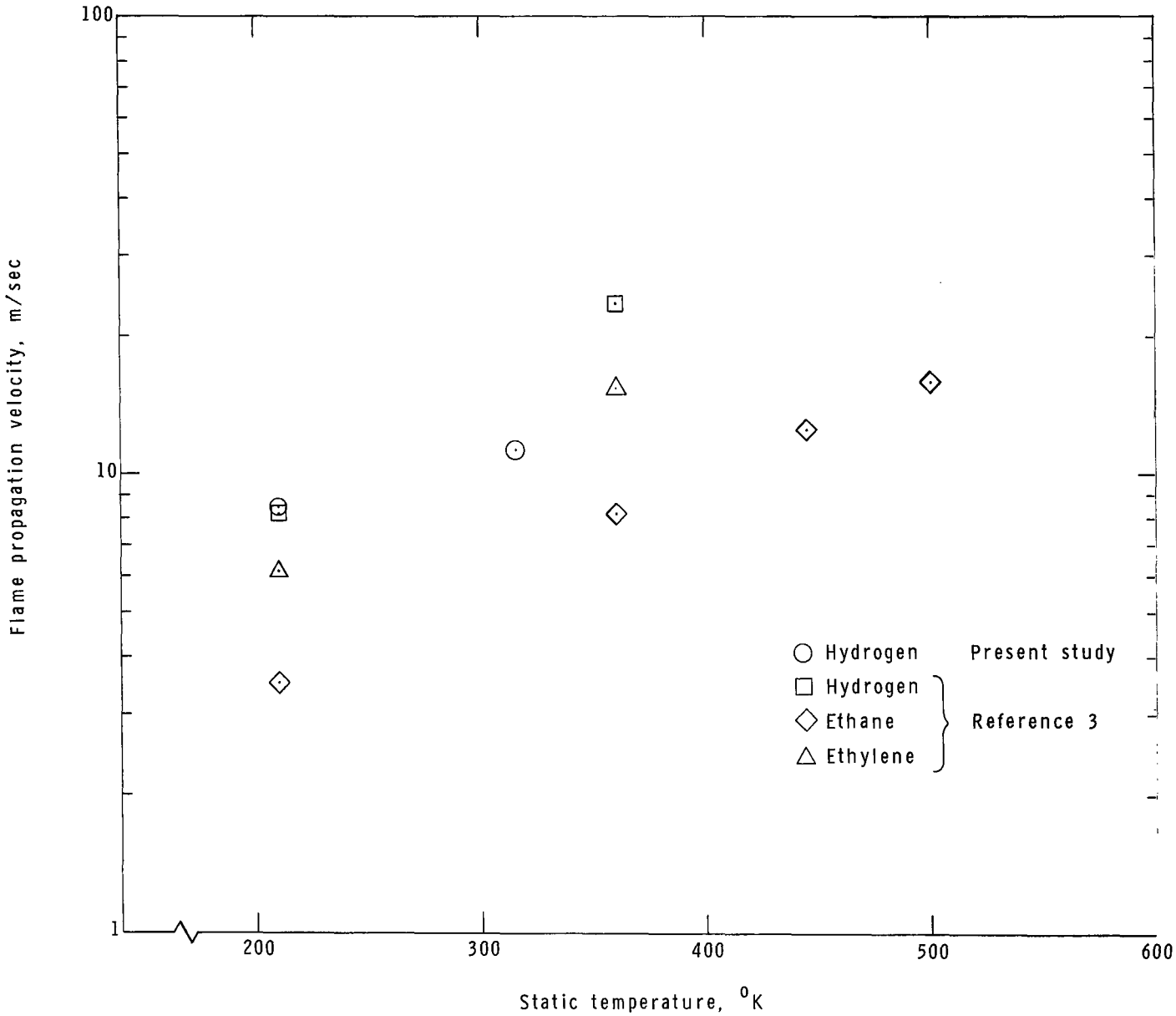

Figure 12.- Flame propagation velocity plotted against initial mixture static temperature for hydrogen, ethane, and ethylene. Mixtures 0.65 stoichiometric.

NATIONAL AERONAUTICS AND SPACE ADMINISTRATION
WASHINGTON, D.C. 20546

OFFICIAL BUSINESS

FIRST CLASS MAIL

POSTAGE AND FEES PAID
NATIONAL AERONAUTICS AND
SPACE ADMINISTRATION

"The aeronautical and space activities of the United States shall be conducted so as to contribute . . . to the expansion of human knowledge of phenomena in the atmosphere and space. The Administration shall provide for the widest practicable and appropriate dissemination of information concerning its activities and the results thereof."

—NATIONAL AERONAUTICS AND SPACE ACT OF 1958

NASA SCIENTIFIC AND TECHNICAL PUBLICATIONS

TECHNICAL REPORTS: Scientific and technical information considered important, complete, and a lasting contribution to existing knowledge.

TECHNICAL NOTES: Information less broad in scope but nevertheless of importance as a contribution to existing knowledge.

TECHNICAL MEMORANDUMS: Information receiving limited distribution because of preliminary data, security classification, or other reasons.

CONTRACTOR REPORTS: Scientific and technical information generated under a NASA contract or grant and considered an important contribution to existing knowledge.

TECHNICAL TRANSLATIONS: Information published in a foreign language considered to merit NASA distribution in English.

SPECIAL PUBLICATIONS: Information derived from or of value to NASA activities. Publications include conference proceedings, monographs, data compilations, handbooks, sourcebooks, and special bibliographies.

TECHNOLOGY UTILIZATION PUBLICATIONS: Information on technology used by NASA that may be of particular interest in commercial and other non-aerospace applications. Publications include Tech Briefs, Technology Utilization Reports and Notes, and Technology Surveys.

Details on the availability of these publications may be obtained from:

SCIENTIFIC AND TECHNICAL INFORMATION DIVISION

NATIONAL AERONAUTICS AND SPACE ADMINISTRATION

Washington, D.C. 20546